International Journal of Recent Technology and Engineering (IJRTE)
ISSN: 2277-3878 (Online), Volume-7, Issue-6, March 2019

Interpretation of Mammogram Images and Shape Description Analysis with Convex Hull Method

Kumara Guru Diderot P, N Vasudevan

Abstract*: Identifying tumour within multiple areas in an image and its morphological feature is one of pioneering areas of mammogram research. Hence, this work interprets the inner shape and features of each mammogram affected regions. The scaling method deployed in this work uses odd series scan which calculates the local connected fractal components with minimal and maximal dimensions. Each image with varying extent of tumour size has been quantitatively scaled in terms of pixel level associating it with its geometrical components. The samples taken for this analysis are being measured with the following affinity of the spatial features and tumour along with the corresponding views. The irregular volume geometry is being converted to fractal dimension using box counting method. Fractal Dimension in Mammogram Images using Convex Hull method (FDMICH) algorithm does not treat the whole image as a single fractal but uses the affected region for quantitative analysis.

Index Terms*: Fractal Dimensions, Computational Geometry and Mammogram.

I. INTRODUCTION

The clustered micro-calcification (MC) appears in thirty to fifty percentages of the diagnosed cases [1]. However, it might be malignant or benign depends on the biopsy or imaging modules. The classification of MC has been further classified in [2] as benign micro-calcification and malignant micro-calcification. The benign MC has smooth shape, clear boundaries with 0.1 to 2.7 mm whereas the shape of malignant MC has no sharp boundaries. The malignant MC is between 0.05 to 0.5m and they are smaller than benign MC [2]. The discussion in [2] has been based on “Micro Computed Tomography” (Micro CT). Though Micro CT has several advantages like it can be rotated in all direction, cross sectional internal structure can be analysed. The disadvantage is it is time consuming for the acquiring and reconstructing the image [3]. The paper is organised where in section 2 deals with literature survey focusing on techniques of mammogram over other image acquiring techniques for breast cancer, its geometrical interpretation and problem definition. Section 3 deals with the development of algorithm focusing on Fractal Dimension in Mammogram Images using Convex Hull method (FDMICH). Section 4 discusses interpretation of results with their corresponding views in mammogram images. Finally, section 5 discusses the consolidation of results.

Revised Manuscript Received on 30 March 2019.
***** Correspondence Author

Kumara Guru Diderot P, Research Scholar, Hindustan Institute of Technology & Science, Chennai, India.

N Vasudevan, Professor, Hindustan Institute of Technology & Science, Chennai, India.

II. LITERATURE SURVEY

Local pathological tissues and its impact of breast cancer have been discussed in [11].They stated that the chemical composition of carbonate content reduction has been found when the benign to malignant with pathological tissues are identified.

The discussion of support vector machine based micro-calcification has been done in [12]. The initial procedure happen the region of interest (ROI) is chosen proceed by morphological enhancement. Followed by segmenting using edge detection algorithms. Finally, “shape”, “texture” and “spectral domain” are used for micro-calcification with suspicious nature.

Breast micro-calcification has been analysed in view level by using a multi view classifier [13]. The view level gets the MLO and CC views followed by “Logistic regression” for each view in determining the stochastic combination of decision..

Computer tomography methods where done in [16] to classify the Ductal Carcinoma In Situ (DCIS) from micro-calcification. The results reveal that malignant calcification associated with DCIS requires more enhancement in images compared with benign calcification.

“Modified Histogram based Adaptive Thresholding” (MHAT) has been proposed in [4] which classifies he micro calcification from masses by using background tissue.

Lymph node (LN) is used to classify micro-calcification in “BI-RADS 3-5” [8] and can be termed as LN positive or LN negative.

The association between calcification and its advancement leading to invasive nature has been discussed in [14]. The finding has been classified with “tumor” relating it to calcification. The tumor scale varies with less than 15 mm to greater than 15 mm [14]. Malignant calcification has been done with combination of Computer Aided Diagnostic (CAD) along with inspection from radiologist [15]. Finding in [15] suggests that more than fifty percentage of the population affected by calcification with invasive cancer can be found out in screening procedure.

Scientific report in [17] states that it micro-calcification might lead to “metastasize” in distant organs and has to be considered with genetic factors.

2.1 Discussion of X-ray mammogram with other techniques

Diffraction Enhanced Imaging (DEI) has been used with analyser crystals which can capture small angle of scatter, refraction compared with the conventional radiography [20].

The detection of calcification using DEI was efficient when the calcification is in spherical or cylindrical shape.

"Photo acoustic mammography" (PAM) has been discussed in [6] wherein the wavelength decides the configuration of the image. The advantage of PAM is it has less exposure to ionizing radiations compared with X-ray mammogram [6]. Micro Pure has been used in [18] which are used for identifying artifacts find more micro calcifications compared with gray scale ultrasound.

Multimodal imaging techniques has been proposed in [19] with micron scale resolution with mineral matrix composition for identifying micro calcification.

X ray tube along with a combination of "Complementary Metal Oxide Semiconductor"(CMOS) and Active Pixel Sensor (APS) [21]. The procedure increases the visibility in findings.

2.2 Geometrical Interpretation of medical images

The discussion of medical images with mathematical methods can be classified as "Mono-Fractal" and "Multi-Fractal" [9]. Mono-Fractal denotes how irregular an object is and the space it occupies. Multi-Fractal is infinite set and it is more complex and wherein a combination of Mono-Fractals may occur. Fractal analysis discussion with MRI Images states the health tissue should occupy more area in the detection window than the foci of concentration [10].Fractal geometry approach based on "self similarity" (structure are associated with one and another) has been discussed in [5] for detection of cancer.

2.3 Problem definition

Bio-signal not being quantified to an absolute scale has to be scaled for proper analysis. In this category the cancerous cell within a corresponding view are subjected to varying dimensions. Fractal geometry is one of the measures which can be used for measuring non integer values with quantifiable scales [22]. Shape of tumour can provide prediction for breast cancer malignancies associated with molecular subtypes [26]. Hence, proper image segmentation is needed.

In order to obtain better delineation in mammogram images discussion were based on isolevel contour with topological representation [23]. Adaptive contour mapping in [24] has been used with the duo of topological and geometrical information. The blurred boundaries proper segmentation has been obtained using this Adaptive contour mapping. Tumour shape classification has been done in [25] with segmented mask and convolution neural network (CNN) which categories labels as "irregular", "lobular", "oval" and "round". The problem is clearly evident anatomical information of breast cancer and its geometrical interpretation has to be analysed with both the brighter and darker regions.

III. ALGORITHM DEVELOPMENT

3.1 Fractal Dimension in Mammogram Images using Convex Hull method (FDMICH)

Methodology:

1. The first step is converting the image to an 8 bit image.
2. Then make the image as binary image.
3. Select the malignant affected region in the binary image with specifying the region of interest then the appropriate x coordinate and y coordinate.
4. Choose the scan type as Odd series.
5. Then select the metrics of convex hull method denoting the region of interest

Circularity can be determined by

$$\text{Circularity} = \frac{4 \times \pi \text{ Area}}{(\text{Perimeter})^2} \quad (1)$$

Span ratio major axis over minor axis of the convex hull.

Hull centre mass is denoted by the X co-ordinates and Y coordinates.

(**MaximumSpan across Hull)** Maximum distance between points in a convex hull denoted in terms of pixels.

(**Radius of curvature (CV) for all Radii**) it can be calculated from circle centre to the points of convex hull. The quantitative metrics for image dimensions are availale in section 4.

IV. RESULTS ANALYSIS

The result of simulations analysis has been carried out using image J software which is being analysed with the Fractal dimensions and Lacunarity plugin. The Fractal dimensions where the metrics of convex hull is used for obtaining the features of image. The assumption is made as the region of interest is known visually.

Table.1The image used for the study and its corresponding data

Figure Number	Age of Patient	Breast density	Right		Left	
			MLO	CC	MLO	CC
The description for Figure 1	51	1	Three abnormalities were found.			
The description for Figure 3	51	1		One Abnormality was found.		
The description for Figure 6	51	1			No Abnormality	
The description for Figure 7	51	1			No Abnormality	
The description for Figure 8	49	1	Six Pathology benign abnormality was found.			
The description for Figure 10	49	1		Six Pathology benign abnormality was found.		
The description for Figure 11	49	1			One Abnormality Pathology Malignant	
The description for Figure 14	49	1				One Abnormality Pathology Malignant

Fig.3 The FORETELL method implementation

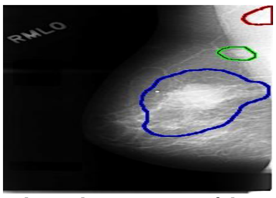

Fig.1 The Right MLO view of the patient

The reason for considering age and breast density because they are the foremost important prediction considered in screening mammogram [7].

There are three abnormalities shown in the figure 1 with red denoting “irregular margin” hidden by other tissues (micro-lobulated). Similarly, the green shows the denoting irregular margin hidden by other tissues (micro-lobulated). Finally the blue color shows “calcification type amorphous distribution clustered”.

Fig.2 Corresponding Binary Image of Right MLO View

The Binary image for Right MLO view is shown in figure 2 the corresponding region of interests is given in Table 1.

Table.2 Region of Interest for Mammogram Image in figure 2

ROI -1	0092-0188
ROI -2	0020-0206
ROI -3	0185-0163

The results discussed in table 3 to table 7 denote the irregular margin and the metrics for convex hull calculations.

Table.3 Results of Convex hull in terms of pixel and axis for ROI-1

Mean foreground pixel	Total pixels	Density = Foreground pixels/ Hull area	Span Ratio
420	924	1.05	1.3205

Table.4 Results of area, perimeter, and circularity, maximum span across hull and centre of mass for ROI 1

Hull’s centre Mass	Maximum Span across Hull	Area	Perimeter	Circularity
188.8604, 91.6168	26.9258	400	73.7718	0.9236

Table.5 Results of width and height of bounding box and metrics of Radii for ROI1

Width of Bounding Rectangle	Height of Bounding Rectangle	Maximum Radius from Hull centre mass	Max/ Min Radii	CV for all Radii
26	23	13.9544	1.4225	0.1151

Table.6 Results of metrics of Radii

Mean Radius	Circle Centre	Diameter of bounding circle	Max/Min Radii from circle’s centre	Min Radii from circle’s centre	CV for all Radii from circle’s centre	Mean radius from circle’s centre
11.8048	18893.5	26.9258	13.4629	1.7344	0.1706	11.8093

Table.7 Method used to calculates is span

Method used to calculate
Span

The results discussed in table 8 to table 12 denote the region of Interest as 0020-0206.

Table.8Results of Convex hull in terms of pixel and axis for ROI-2

Mean foreground pixel	Total pixels	Density = Foreground pixels/ Hull area	Span Ratio
438	620	1.0842	1.5921

Table.9 Results of area, perimeter, circularity, maximum span across hull and centre of mass for ROI 2

Hull’s centre Mass	Maximum Span across Hull	Area	Perimeter	Circularity
207.17, 22.5453	32.2025	404	82.8128	0.7403

Table.10 Results of width and height of bounding box and metrics of Radii for ROI2

Width of Bounding Rectangle	Height of Bounding Rectangle	Maximum Radius from Hull centre mass	Max/ Min Radii	CV for all Radii
19	32	19.2132	1.8327	0.2083

Table.11 Results of metrics of Radii for ROI-2

Mean Radius	Circle Centre	Diameter of bounding circle	Max/Min Radii from circle’s centre	Min Radii from circle’s centre	CV for all Radii from circle’s centre	Mean radius from circle’s centre
13.9436	20819.5	32.2025	16.1012	1.6856	0.1515	14.1693

Table.12The method used to calculates is span

Method used to calculate
Span

The results discussed in table 13 to table 17 denote the0185-0163.

Table.13Results of Convex hull in terms of pixel and axis for ROI-3

Mean foreground pixel	Total pixels	Density = Foreground pixels/ Hull area	Span Ratio
8308	12400	0.966	1.4791

Table.14Results of area, perimeter, circularity, maximum span across hull and centre of mass for ROI 3

Hull’s centre Mass	MaximumSpan across Hull	Area	Perimeter	Circularity
156.939,182.257	129.0969	8600	347.2956	0.896

Table.15Results of width and height of bounding box and metrics of Radii for ROI-3

Width of Bounding Rectangle	Height of Bounding Rectangle	Maximum Radius from Hull centre mass	Max/ Min Radii	CV for all Radii
99	125	69.2171	1.5757	0.141

Table.16 Results of metrics of Radii for ROI-3

Mean Radius	Circle Centre	Diameter of bounding circle	Max/Min Radii from circle's centre	Min Radii from circle's centre	CV for all Radii from circle's centre	Mean radius from circle's centre
55.8316	155.1345, 186.5054	129.2679	64.634	1.5339	0.1497	56.1454

Table.17 Method used to calculate is Triangle

Method used to calculate
Triangle

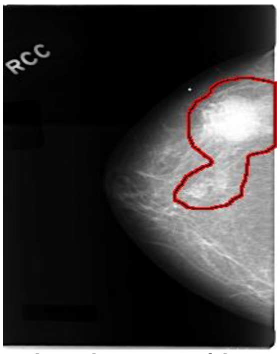

Fig.3 The Right CC view of the patient

There is only one type of abnormality shown in the figure 3 with red color. The lesion types are "irregular margin microlobulated" as well as calcification type amorphous distribution clustered.


Fig.4 Corresponding Binary Image of Right CC View

The Binary image for Right CC view is shown in figure 4 the corresponding region of interests is given in Table 18.

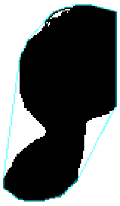
Fig.5 Convex Hull Image of Right CC view

Table.18 Region of Interest for Mammogram Image in figure 4

ROI -1	0144-0172

The results discussed in table 19 to table 23denote the Region of Interest for Figure 5.

Table.19 Results of Convex hull in terms of pixel and axis for ROI-1

Mean foreground pixel	Total pixels	Density = Foreground pixels/ Hull area	Span Ratio
6678	10395	0.8723	2.1521

Table.20 Results of area, perimeter, circularity, maximum span across hull and centre of mass for ROI 1

Hull's centre Mass	Maximum Span across Hull	Area	Perimeter	Circularity
27.9563, 81.8652	144.0139	7656	351.3243	0.7795

Table.21Results of width and height of bounding box and metrics of Radii for ROI-1

Width of Bounding Rectangle	Height of Bounding Rectangle	Maximum Radius from Hull centre mass	Max/ Min Radii	CV for all Radii
76	136	90.3372	1.9891	0.2548

Table.22Results of metrics of Radii for ROI-1

Mean Radius	Circle Centre	Diameter of bounding circle	Max/Min Radii from circle's centre	Min Radii from circle's centre	CV for all Radii from circle's centre	Mean radius from circle's centre
64.123	43.8012, 69.8975	144.0146	72.0073	2.169	0.1651	62.8194

Table.23 Method used to calculate is Span

Method used to calculate
Span

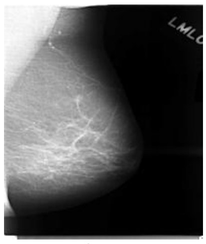
Fig.6 The Left MLO view of the patient with no abnormality

No abnormalities are found in the left MLO view in figure 3 and left CC view in figure 4.

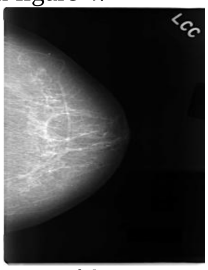

Fig.7 The Left CC view of the patient with no abnormality

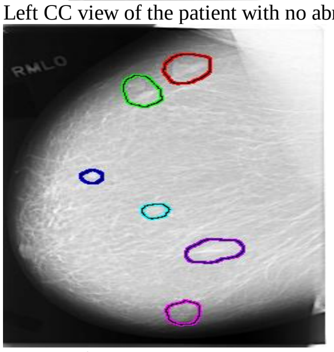

Fig.8 Right MLO view of the patient is shown with six abnormalities

The six lesions shown in figure 8 all of which are margins are circumscribed in the right MLO view.

Fig.9 Binary Image of Right MLO view with six abnormalities

Table.24 Region of Interest for Mammogram Image in figure 9

ROI -1	0329-0135
ROI -2	0259-0159
ROI -3	0213-0114
ROI -4	0174-0066
ROI -5	0076-0105
ROI -6	0051-0138

The results discussed in table 25 to table 29 denote the Region of Interest for affected region in figure 9.

Table.25 Results of Convex hull in terms of pixel and axis for ROI-1 to ROI6

Region of Interest	Mean foreground pixel	Total pixels	Density = Foreground pixels/ Hull area	Span Ratio
ROI-1	729	960	1.0311	1.2312
ROI-2	591	858	1.019	1.3635
ROI-3	104	156	1.1183	1.1146
ROI-4	222	285	1.0725	1.2817
ROI-5	805	1232	1.0216	1.8107
ROI-6	391	624	0.8537	1.0815

Table.26 Results of area, perimeter, circularity, maximum span across hull and centre of mass for ROI 1 to ROI-6

Region of Interest	Hull's centre Mass	Maximum Span across Hull	Area	Perimeter	Circularity
ROI-1	15.9935,14.1032	34.6554	707	96.6811	0.9505
ROI-2	11.9464,16.6986	32.5576	580	88.6496	0.9274
ROI-3	6.5667, 5.9111	12.1655	93	35.1062	0.9483
ROI-4	9.1584, 6.9455	18.4391	207	52.2068	0.9544
ROI-5	21.4339,13.386	42.72	788	107.4669	0.8574
ROI-6	12.0266,11.3459	25.807	458	77.7286	0.9526

Table.27 Results of width and height of bounding box and metrics of Radii for ROI-1 to ROI- 6

Region of Interest	Width of Bounding Rectangle	Height of Bounding Rectangle	Maximum Radius from Hull centre mass	Max/ Min Radii	CV for all Radii
ROI-1	31	31	18.0906	1.4211	0.09
ROI-2	25	34	17.1586	1.4388	0.1022
ROI-3	12	13	6.6296	1.2861	0.0811
ROI-4	18	16	9.3628	1.3297	0.0956
ROI-5	41	27	21.4777	1.8471	0.196
ROI-6	23	27	14.5316	1.4295	0.0972

Table.28 Results of metrics of Radii

Region of Interest	Mean Radius	Circle Centre	Diameter of bounding circle	Max/Min Radii from circle's centre	CV for all Radii from circle's centre	Mean radius from circle's centre
ROI-1	15.4653	17.2685,14.7172	34.8375	1.5191	0.1064	15.677
ROI-2	14.4029	11,16	32.5576	1.4799	0.1146	14.3571
ROI-3	5.7049	6.0833,5.5	12.2077	1.3187	0.0853	5.61
ROI-4	8.3055	9.0645,6.2903	18.4487	1.4459	0.0991	8.3575
ROI-5	17.5445	21.5,14	42.72	1.9398	0.1972	17.5437
ROI-6	12.6531	12.6688,12.8766	25.9826	1.2037	0.0525	12.5194

Table.29 The method used to calculate is Triangle

Region of Interest	Method used to calculate
ROI-1	Triangle
ROI-2	Span
ROI-3	Span
ROI-4	Triangle
ROI-5	Span
ROI-6	Triangle

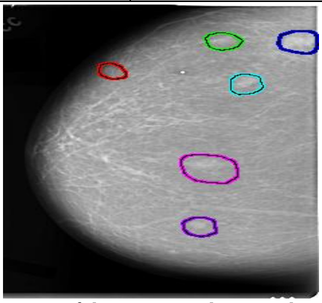

Fig.10 Right CC view of the patient is shown with six abnormalities

The six lesions shown in figure 10 are margins are circumscribed in the right CC view. Both in figure 8 and figure 10 the mass shape is said to be oval.

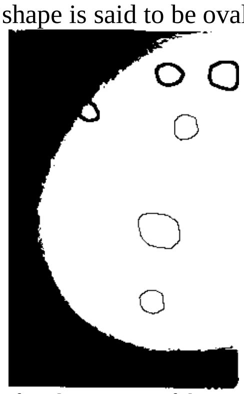

Fig.11 Binary Image of Right CC view of the patient is shown with six abnormalities

Table.29 Region of Interest for Mammogram Image in figure 9

ROI -1	0279-0146
ROI -2	0206-0153
ROI -3	0084-0082
ROI -4	0100-0181
ROI -5	0046-0164
ROI -6	0047-0219

Table.30 Results of Convex hull in terms of pixel and axis for ROI-1 to ROI6

Region of Interest	Mean foreground pixel	Total pixels	Density = Foreground pixels/ Hull area	Span Ratio
ROI-1	383	528	1.0464	1.0529
ROI-2	1095	1435	1.0282	1.3292
ROI-3	140	256	1.0606	1.1567
ROI-4	415	552	1.0533	1.0592
ROI-5	283	414	1.0639	1.2917
ROI-6	471	625	1.0584	1.0625

The results discussed in table 30 to table 34 denote the region of Interest as

Table.31 Results of area, perimeter, circularity, maximum span across hull and centre of mass for ROI 1 to ROI-6

Region of Interest	Hull's centre Mass	Maximum Span across Hull	Area	Perimeter	Circularity
ROI-1	11.7431,10.2541	23.7065	366	69.1578	0.9616
ROI-2	20.0606,16.1032	43.909	1065	119.3126	0.9401
ROI-3	7.3976, 7.8386	14.4222	132	42.3809	0.9235
ROI-4	10.2442,11.27	24.4131	394	71.9196	0.9572
ROI-5	10.2854,8.2165	21.3776	266	59.2077	0.9535
ROI-6	12.5636,11.2181	26.4008	445	77.6636	0.9271

Table.32 Results of width and height of bounding box and metrics of Radii for ROI-1 to ROI- 6

Region of Interest	Width of Bounding Rectangle	Height of Bounding Rectangle	Maximum Radius from Hull centre mass	Max/ Min Radii	CV for all Radii
ROI-1	21	23	11.9591	1.1455	0.0362
ROI-2	39	35	22.5786	1.4209	0.1126
ROI-3	13	16	7.8487	1.3011	0.08
ROI-4	21	24	12.4146	1.1516	0.0457
ROI-5	21	18	10.7834	1.3286	0.0993
ROI-6	23	25	13.6901	1.315	0.0624

Table.33 Results of metrics of Radii

Region of Interest	Mean Radius	Circle Centre	Diameter of bounding circle	Max/Min Radii from circle's centre	Min Radii from circle's centre	CV for all Radii from circle's centre	Mean radius from circle's centre
ROI-1	11.0935	11.5,10.5	23.7065	11.8533	1.1708	0.0428	11.0999
ROI-2	18.8583	20,15	43.909	21.9545	1.4678	0.1142	18.7987
ROI-3	6.7836	7.5,7.4091	14.8519	7.4259	1.3191	0.0838	6.7868
ROI-4	11.5252	10.4118,11.5882	24.4553	12.2277	1.1678	0.0609	11.4915
ROI-5	9.512	10.5,7	21.3776	10.6888	1.5388	0.1362	9.0552
ROI-6	12.6967	12.7,11.5	26.7686	13.3843	1.3128	0.0642	12.6829

Table.34 The method used to calculate is Triangle

Region of Interest	Method used to calculate
ROI-1	Span
ROI-2	Span
ROI-3	Triangle
ROI-4	Triangle
ROI-5	Span
ROI-6	Triangle

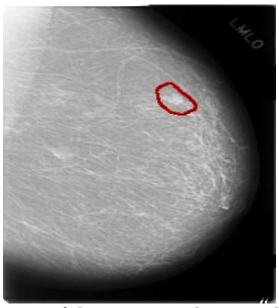

Fig.11 Left MLO view of the patient is shown with one abnormality

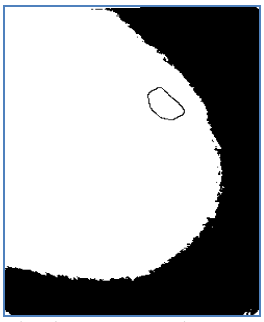

Fig.12 Binary Image of Left MLO view of the patient is shown with one abnormality

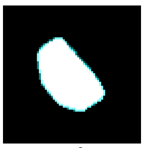

Fig.13 Segmented Region of Interest taken for analysis

Table.35 Region of Interest for Mammogram Image in figure 13

ROI -1	0115-0155

The results discussed in table 36 to table 40 denote the region of Interest as

Table.36 Results of Convex hull in terms of pixel and axis for ROI-1

Mean foreground pixel	Total pixels	Density = Foreground pixels/ Hull area	Span Ratio
772	1258	1.0252	1.6845

Table.37 Results of area, perimeter, circularity, maximum span across hull and centre of mass for ROI 1

Hull's centre Mass	Maximum Span across Hull	Area	Perimeter	Circularity
15.3048,19.352	39.2046	753	104.9485	0.8591

Table.38Results of width and height of bounding box and metrics of Radii for ROI1

Width of Bounding Rectangle	Height of Bounding Rectangle	Maximum Radius from Hull centre mass	Max/ Min Radii	CV for all Radii
33	38	20.3531	1.6106	0.1564

Table.39 Results of metrics of Radii

Mean Radius	Circle Centre	Diameter of bounding circle	Maximum Radii from circle's centre	Max/Min Radii from circle's centre	CV for all Radii from circle's centre	Mean radius from circle's centre
17.0523	16.5,18	39.2046	19.6023	1.7045	0.1303	17.9211

Table.40 Method used to calculates is span

Method used to calculate
Span

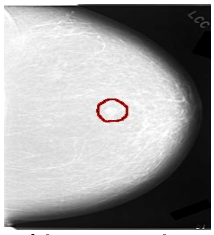

Fig.14 Left MLO view of the patient is shown with one abnormality

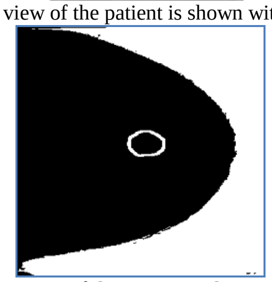

Fig.15 The Left MLO view of the patient is shown with one abnormality

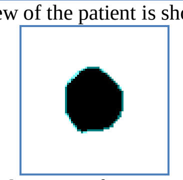

Fig.16 Segmented Region of Interest taken for analysis

Table.41 Region of Interest for Mammogram Image in figure 9

ROI -1	0172-0121

The results discussed in table 42 to table 46denote the Region of Interest as in figure 9.

Table.42 Results of Convex hull in terms of pixel and axis for ROI-1

Mean foreground pixel	Total pixels	Density = Foreground pixels/ Hull area	Span Ratio
734	1404	1.0309	1.1075

Table.43 Results of area, perimeter, circularity, maximum span across hull and centre of mass for ROI 1

Hull's centre Mass	Maximum Span across Hull	Area	Perimeter	Circularity
9.5, 7.6429	32.9848	712	96.365	0.9635

Table.44 Results of width and height of bounding box and metrics of Radii for ROI1

Width of Bounding Rectangle	Height of Bounding Rectangle	Maximum Radius from Hull centre mass	Max/ Min Radii	CV for all Radii
28	34	29.992	9.8695	0.4695

Table.45 Results of metrics of Radii

Mean Radius	Circle Centre	Diameter of bounding circle	Maximum Radii from circle's centre	Max/Min Radii from circle's centre	CV for all Radii from circle's centre	Mean radius from circle's centre
19.6705	16.6316,19.1579	33.0105	16.5053	1.186	0.0574	15.5609

Table.46 Method used to calculates is span

Method used to calculate
Span

V. CONCLUSION

Recognition of varying types of cancerous cells within a mammogram image and its corresponding view has been estimated by this work. By properly segmenting the region of interest of cancerous cells the notions required for determining the spatial coordinates can be measured. The proposed work uses convex hull algorithm for identifying the set of point with the morphological features of a mammogram affected region within an image. Difference in pixel intensity measures provide additional computed values across the inner boundaries of mammogram infected image. Sampling pixel by pixel gives more precise descriptions shown in terms of varying metrics like circularity, radii. Future work will focus on noise removal and detecting cancer stages with classifiers from mammogram images.

REFERENCES

1. Wei, L., Yang, Y., Nishikawa, R. M., & Jiang, Y. (2005). A study on several machine-learning methods for classification of malignant and benign clustered microcalcifications. IEEE transactions on medical imaging, 24(3), 371-380.
2. Gufler, H., Wagner, S., & Franke, F. E. (2011). The interior structure of breast microcalcifications assessed with micro computed tomography. ActaRadiologica, 52(6), 592-596.
3. Tang, R., Buckley, J. M., Fernandez, L., Coopey, S., Aftreth, O., Michaelson, J., ... & Yagi, Y. (2013). Micro-computed tomography (Micro-CT): a novel approach for intraoperative breast cancer specimen imaging. Breast cancer research and treatment, 139(2), 311-316.
4. Patel, B. C., Sinha, G. R., &Soni, D. (2019). Detection of masses in mammographic breast cancer images using modified histogram based adaptive thresholding (MHAT) method. International Journal of Biomedical Engineering and Technology, 29(2), 134-154.
5. Nayak, S. R., & Mishra, J. (2019). Analysis of Medical Images Using Fractal Geometry. In Histopathological Image Analysis in Medical Decision Making (pp. 181-201). IGI Global.
6. Heijblom, M., Piras, D., Xia, W., van Hespen, J. C., Klaase, J. M., Van den Engh, F. M., ... & Manohar, S. (2012). Visualizing breast cancer using the Twente photoacoustic mammoscope: what do we learn from twelve new patient measurements?. Optics express, 20(11), 11582-11597.
7. Carney, P. A., Miglioretti, D. L., Yankaskas, B. C., Kerlikowske, K., Rosenberg, R., Rutter, C. M., & Cutter, G. (2003). Individual and combined effects of age, breast density, and hormone replacement therapy use on the accuracy of screening mammography. Annals of internal medicine, 138(3), 168-175.
8. Cen, D., Xu, L., Zhang, S., Zhou, S., Huang, Y., Chen, Z., & Wang, Q. (2017). BI-RADS 3–5 microcalcifications: prediction of lymph node metastasis of breast cancer. Oncotarget, 8(18), 30190.
9. Ţălu, Ş. (2012). Mathematical methods used in monofractal and multifractal analysis for the processing of biological and medical data and images. ABAH Bioflux, 4(1), 1-4.
10. Marusina, M. Y., Mochalina, A. P., Frolova, E. P., Satikov, V. I., Barchuk, A. A., Kuznetcov, V. I., &Tarakanov, S. A. (2017). MRI image processing based on fractal analysis. Asian Pacific journal of cancer prevention: APJCP, 18(1), 51.
11. Baker, R., Rogers, K. D., Shepherd, N., & Stone, N. (2010). New relationships between breast microcalcifications and cancer. British journal of cancer, 103(7), 1034.
12. Singh, S., Kumar, V., Verma, H. K., & Singh, D. (2006, August). SVM based system for classification of microcalcifications in digital mammograms. In Engineering in Medicine and Biology Society, 2006. EMBS'06. 28th Annual International Conference of the IEEE (pp. 4747-4750). IEEE.
13. Bekker, A. J., Shalhon, M., Greenspan, H., & Goldberger, J. (2016). Multi-view probabilistic classification of breast microcalcifications. IEEE Transactions on medical imaging, 35(2), 645-653.
14. Nyante, S. J., Lee, S. S., Benefield, T. S., Hoots, T. N., & Henderson, L. M. (2017). The association between mammographic calcifications and breast cancer prognostic factors in a populationbased registry cohort. Cancer, 123(2), 219-227.
15. Mordang, J. J., Gubern-Mérida, A., Bria, A., Tortorella, F., Mann, R. M., Broeders, M. J. M., &Karssemeijer, N. (2018). The importance of early detection of calcifications associated with breast cancer in screening. Breast cancer research and treatment, 167(2), 451-458.
16. Aminololama S, S., Abbey, C. K., Gazi, P., Prionas, N. D., Nosratieh, A., Li, C. S., & Lindfors, K. K. (2016). Differentiation of ductal carcinoma in-situ from benign micro-calcifications by dedicated breast computed tomography. European journal of radiology, 85(1), 297-303.
17. Rizwan, A., Paidi, S. K., Zheng, C., Cheng, M., Barman, I., &Glunde, K. (2018). Mapping the genetic basis of breast microcalcifications and their role in metastasis. Scientific reports, 8.
18. Machado, P., Eisenbrey, J. R., Cavanaugh, B., & Forsberg, F. (2012). New image processing technique for evaluating breast microcalcifications: a comparative study. Journal of Ultrasound in Medicine, 31(6), 885-893.
19. Kunitake, J. A., Choi, S., Nguyen, K. X., Lee, M. M., He, F., Sudilovsky, D., &Fratzl, P. (2018). Correlative imaging reveals physiochemical heterogeneity of microcalcifications in human breast carcinomas. Journal of structural biology, 202(1), 25-34.
20. Kiss, M. Z., Sayers, D. E., Zhong, Z., Parham, C., & Pisano, E. D. (2004). Improved image contrast of calcifications in breast tissue specimens using diffraction enhanced imaging. Physics in Medicine & Biology, 49(15), 3427.
21. Koukou, V., Martini, N., Fountos, G., Michail, C., Sotiropoulou, P., Bakas, A., &Nikiforidis, G. (2017). Dual energy subtraction method for breast calcification imaging. Nuclear Instruments and Methods in Physics Research Section A: Accelerators, Spectrometers, Detectors and Associated Equipment, 848, 31-38.
22. Klonowski, W. (2000). Signal and image analysis using chaos theory and fractal geometry. Machine Graphics and Vision, 9(1/2), 403-432.
23. Hong, B. W., &Sohn, B. S. (2010). Segmentation of regions of interest in mammograms in a topographic approach. IEEE Transactions on Information Technology in Biomedicine, 14(1), 129-139.
24. Kim, J., Park, B. Y., Akram, F., Hong, B. W., & Choi, K. (2013). Multipass active contours for an adaptive contour map. Sensors, 13(3), 3724-3738.
25. Singh, V. K., Romani, S., Rashwan, H. A., Akram, F., Pandey, N., Sarker, M. M. K., & Arenas, M. (2018, September). Conditional Generative Adversarial and Convolutional Networks for X-ray Breast Mass Segmentation and Shape Classification. In International Conference on Medical Image Computing and Computer-Assisted Intervention (pp. 833-840). Springer, Cham.
26. Tamaki, K., Ishida, T., Miyashita, M., Amari, M., Ohuchi, N., Tamaki, N., &Sasano, H. (2011). Correlation between mammographic findings and corresponding histopathology: potential predictors for biological characteristics of breast diseases. Cancer science, 102(12), 2179-2185.